MATERIALS SCIENCE

High-performance subambient radiative cooling enabled by optically selective and thermally insulating polyethylene aerogel

A. Leroy[1], B. Bhatia[1], C. C. Kelsall[1], A. Castillejo-Cuberos[2,3], M. Di Capua H.[2,3,4], L. Zhao[1], L. Zhang[1], A. M. Guzman[2,3,4], E. N. Wang[1]*

Recent progress in passive radiative cooling technologies has substantially improved cooling performance under direct sunlight. Yet, experimental demonstrations of daytime radiative cooling still severely underperform in comparison with the theoretical potential due to considerable solar absorption and poor thermal insulation at the emitter. In this work, we developed polyethylene aerogel (PEA)—a solar-reflecting (92.2% solar weighted reflectance at 6 mm thick), infrared-transparent (79.9% transmittance between 8 and 13 μm at 6 mm thick), and low-thermal-conductivity (k_{PEA} = 28 mW/mK) material that can be integrated with existing emitters to address these challenges. Using an experimental setup that includes the custom-fabricated PEA, we demonstrate a daytime ambient temperature cooling power of 96 W/m^2 and passive cooling up to 13°C below ambient temperature around solar noon. This work could greatly improve the performance of existing passive radiative coolers for air conditioning and portable refrigeration applications.

INTRODUCTION

Subambient cooling is vital for minimizing food shortage, promoting human well-being, and driving sustainable economic growth (*1*). Lack of and inadequate refrigeration of perishable food products in developing countries are still responsible for more than 40% of postharvest food spoilage, leading to unnecessary greenhouse gas emissions, biodiversity and habitat loss, as well as water consumption (*2*). Moreover, air conditioning use in buildings is poised to surge in hotter parts of the world with growing populations and economic activity, further increasing the world's energy consumption and CO_2 emissions (*1*). Fortunately, passive, affordable, and more efficient cooling solutions have the potential to reduce food spoilage as well as meet space cooling energy needs without any CO_2 emissions. One approach that has generated notable interest in recent years is radiative cooling (*3*–*23*)—a passive cooling solution that relies on the natural emission of infrared (IR) radiation of terrestrial objects to the cold (3 K) outer space through the IR-transparent window of the atmosphere (8 to 13 μm).

By radiatively rejecting heat to space, radiative cooling theoretically has the potential to passively cool down a surface (emitter) facing the sky to more than ~50°C below ambient temperature and achieve cooling power P_{cool} >100 W/m^2 at ambient temperature (*12*). However, experimentally achieving subambient cooling or substantial cooling power under direct sunlight [global horizontal irradiance (GHI) I_{sun} ~1000 W/m^2] has proven challenging because of high solar absorption [$P_{sun} = (1 - R_{solar})I_{sun}$] and parasitic heat gain [$P_{parasitic} = h_{eff}(T_{amb} - T_{emitter})$]—respectively characterized by the solar reflectivity R_{solar} of the emitter and the effective heat transfer coefficient h_{eff} between the emitter at temperature $T_{emitter}$ and its environment at T_{amb}. The influence of R_{solar} and h_{eff} on the radiative cooling power is shown in fig. S1.

Recent work on passive daytime radiative cooling has made remarkable progress in the design of emitters, demonstrating high solar reflectivity (R_{solar} = 94 to 99%) as well as high mid-IR emissivity (ε_{IR} = 60 to 97%) that has enabled cooling up to 10.6°C below ambient temperature under direct sunlight (*19*). These performance enhancements were achieved primarily through the proposed use of one-dimensional (1D) (*9*, *12*, *14*), 2D (*11*, *24*), and 3D (*8*) photonic structures, metamaterials (*7*, *13*, *19*), hierarchically porous polymeric materials (*22*), pigmented paints (*4*), and even gases such as C_2H_4 (*5*) and NH_3 (*6*). In addition, several approaches to reduce the parasitic heat transfer $P_{parasitic}$ between the cold emitter and its warmer surrounding environment have been proposed. These include a vacuum chamber to suppress convection heat transfer, which enabled a record-low h_{eff} = 0.2 to 0.3 W/m^{2}K (*12*, *25*), although at the expense of cost and scalability. More robust, scalable, and cheaper solutions have also been proposed that rely on using IR-transparent convection covers such as thin polyethylene films (*4*–*6*, *9*, *11*, *15*, *17*, *19*), corrugated structures (*26*), and meshes (*27*), as well as ZnSe (*28*), CdS (*29*), Ge (*25*), or Si (*25*) windows placed over the emitter. Despite the recent advances, solar absorption still induces a 10 to 60% reduction in cooling power at peak solar irradiance (i.e., 10 to 60 W/m^2 out of the ~100 W/m^2). In addition, high parasitic heat gain (typical h_{eff} = 3 to 10 W/m^{2}K for nonvacuum systems) rapidly becomes dominant at subambient temperatures, limiting the minimum achievable temperature to only ~10°C below ambient.

While most of the previous work has focused on reducing either solar absorption or parasitic heat gain, a solution that addresses both could enable simpler and higher performance radiative cooling. To tackle this challenge, we propose using an optically selective and thermally insulating (OSTI) emitter cover, as presented in Fig. 1 (*18*, *20*). By taking advantage of the cover's added thermal conduction resistance between the emitter and the ambient (i.e., reduced h_{eff}), as well as its selective reflectance and transmittance (i.e., high solar reflectivity R_{solar} and IR transmittance $\tau_{8-13\mu m}$), higher subambient cooling power and colder stagnation temperatures may be achieved. Inspired by this approach, we theoretically and experimentally demonstrate

[1]Department of Mechanical Engineering, Massachusetts Institute of Technology, Cambridge, MA 02139, USA. [2]Centro de Energía, Escuela de Ingeniería, Pontificia Universidad Católica de Chile, Vicuña Mackenna 4860, Santiago, Chile. [3]Departamento de Ingeniería Mecánica y Metalúrgica, Pontificia Universidad Católica de Chile, Vicuña Mackenna 4860, Santiago, Chile. [4]Micro and Nanofluidics Laboratory for Life Sciences, Pontificia Universidad Católica de Chile, Vicuña Mackenna 4860, Santiago, Chile.
*Corresponding author. Email: enwang@mit.edu

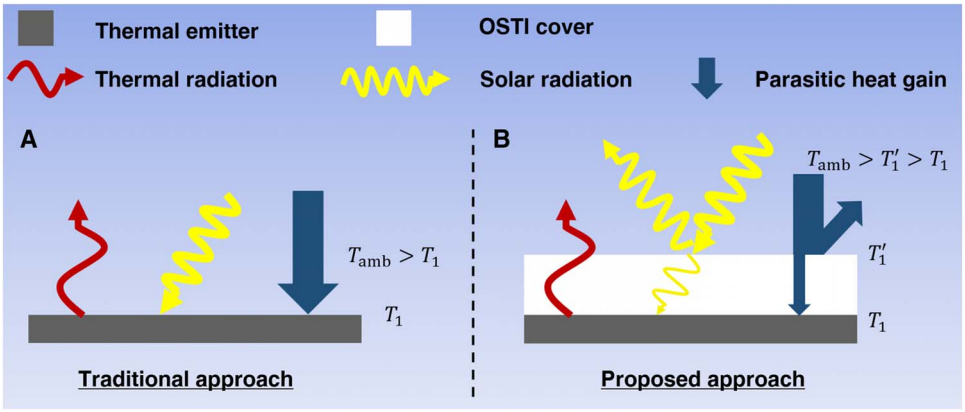

Fig. 1. Schematic of the proposed approach. (**A**) Traditional approach to radiative cooling. An emitter facing the sky is exposed to solar irradiation and parasitic heat gain from the ambient air due to convection. (**B**) Proposed approach where an OSTI cover is placed on top of the emitter. This insulation reduces parasitic heat gain as well as the solar irradiation reaching the emitter, enabling lower emitter temperatures and higher subambient cooling power.

deep subambient radiative cooling using custom-fabricated polyethylene aerogel (PEA), a thermally insulating, solar-reflecting, and IR-transmitting material. We first report the fabrication and corresponding optical and thermal properties of PEA. Using experimentally determined optical properties of the fabricated PEA and a robust theoretical model that accounts for radiative and conductive transport within the PEA, we then show that the approach has the potential to achieve subambient cooling of up to 7°C under 1000 W/m^2 of direct sunlight and U.S. Standard Atmosphere 1976 (*30*), beating a selective emitter alone by more than 4°C. We also demonstrate that using PEA enables the use of simpler emitters due to the optical selectivity of the cover while opening up a wide regime of subambient temperatures and cooling powers that were not previously achievable. Last, using a proof-of-concept experimental setup and the fabricated PEA, we report a maximum ambient temperature daytime cooling power of 96 W/m^2 and a subambient cooling as high as 13°C around solar noon (1123 W/m^2 GHI), a more than 22% increase in emitter subcooling under direct sunlight over previously reported work (*19*) operating under similar experimental conditions (around solar noon under direct sunlight or without a solar shade casting a shade on the emitter and in air). These theoretical and experimental results demonstrate the potential of OSTI covers for simple and high-performance radiative cooling, which could improve the performance of existing radiative coolers as well as enable next-generation passive cooling systems.

RESULTS

Polyethylene aerogel

In past work, thin (<100 μm) polyethylene (*31*) and nanoporous polyethylene (*32*) films have been widely used as convection covers because of their low cost and good IR transmittance. However, their high density has precluded the use of thicker films that could provide additional thermal insulation to the emitter due to dominant IR absorption. By combining the advantages of polyethylene with that of aerogels, a class of materials with high porosity, ultralow thermal conductivity, and density, PEA could thus offer the possibility of a highly insulating and IR-transparent cover for radiative cooling.

Our PEA fabrication used a process based on the thermally induced phase separation (TIPS) of a homogeneous polyethylene/paraffin oil mixture (*33*, *34*), followed by a solvent extraction by supercritical point drying. By controlling the initial polymer concentration, the TIPS process allowed us to create a highly porous (>0.9), low-density (~10 kg/m^3), and highly IR-transparent and solar-reflecting material, while the critical point drying enabled solvent extraction without damaging the porous structure. More details on the fabrication of PEA are given in Materials and Methods.

The optical and thermal properties of our custom-fabricated PEA are key to its application as an OSTI cover for radiative cooling. Figure 2A shows an image of a representative PEA sample, 10 cm in diameter and 6 mm thick, along with a scanning electron microscopy (SEM) image of its internal porous structure. Owing to its highly porous structure and low density (14 ± 2 kg/m^3), our PEA has a low thermal conductivity of 28 ± 5 mW/mK, nearly equal to that of air (k_{air} = 26 mW/mK) due to negligible solid heat transfer through the polymer (see Materials and Methods for more details on the custom guarded-hot-plate steady-state thermal conductivity setup used for thermal characterization). The optical reflectance and transmittance of the 6-mm-thick PEA sample are also shown in Fig. 2B, along with the air mass 1.5 (AM1.5) solar spectrum and a standard atmospheric transmittance (U.S. Standard Atmosphere 1976). The results show that in the atmospheric transparency spectral window (8 to 13 μm), the PEA has high transmittance ($\tau_{8-13\mu m}$ = 0.799). However, the PEA sample is strongly scattering at shorter wavelengths (0.3 to 2.5 μm) because of its porous structure, resulting in high reflectance of solar irradiation (R_{solar} = 0.922). Strong absorption peaks at 3.5, 6.8, and 13.8 μm, characteristic to polyethylene, are due to asymmetric stretching, bending, and wagging of CH_2 molecules (*31*). Because of its characteristic porous structure and ultralow density, PEA has exceptional optical and thermal properties, ideal for high-performance subambient radiative cooling, even at large thicknesses (~cm), which was not possible with previous materials such as nanoporous polyethylene (*32*).

Modeling the cooling potential of an emitter coupled with PEA

To accurately evaluate the performance of an emitter coupled with PEA, both conductive and radiative thermal transport must be simultaneously considered. The thicker the PEA, the more it absorbs, emits, and scatters light, which, in turn, affects the temperature profile within it and the corresponding conductive heat flux (i.e., parasitic heat gain $P_{parasitic}$). The contribution of the conductive and radiative heat fluxes as well as their interactions therefore affect the total heat flux at the emitter (i.e., emitter cooling power P_{cool}). To account for both effects,

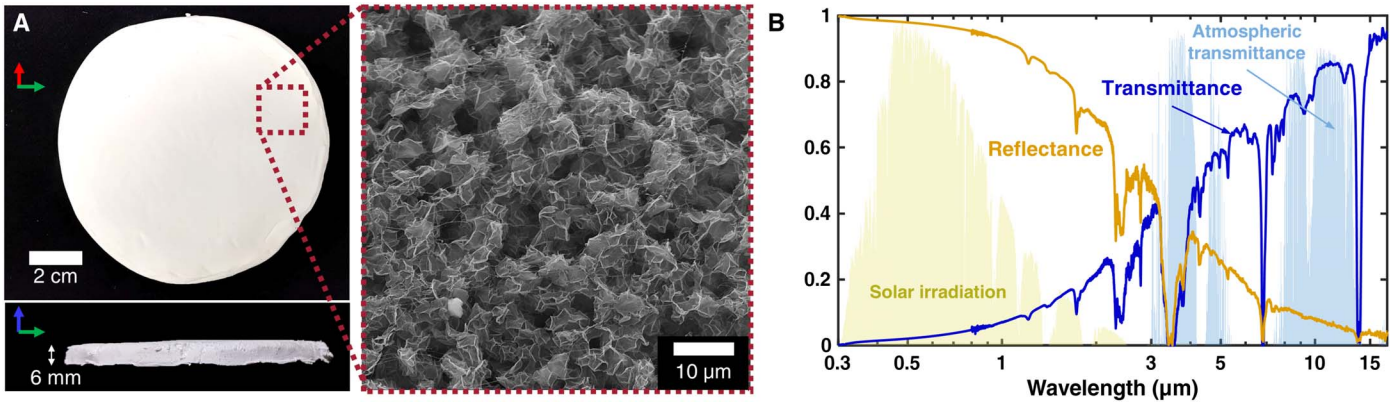

Fig. 2. Polyethylene aerogel. (**A**) Image of a 10-cm-diameter and 6-mm-thick PEA sample. The inset shows an SEM image at a magnification of ×1500. Photo credit: Arny Leroy, Massachusetts Institute of Technology. (**B**) Hemispherical transmittance and reflectance of a 6-mm-thick PEA sample along with the normalized AM1.5 solar spectrum and the atmospheric transmittance (U.S. Standard Atmosphere 1976).

we numerically solved the steady-state 1D heat transfer equation (HTE) within the PEA

$$-k_{\mathrm{PEA}}\frac{d^2T}{dx^2}+\frac{dq_{\mathrm{r}}}{dx}=0 \quad (1)$$

where k_{PEA} is the PEA thermal conductivity, x is the spatial coordinate along the thickness of the PEA, T is the spatial PEA temperature profile, and q_{r} is the spatial radiative heat flux. The simplified HTE (Eq. 1) states that for energy to be conserved, the spatial rate of change of the conductive and radiative heat flux are of equal magnitude (but of different sign). Whereas the conductive term can easily be calculated from Fourier's law, the evaluation of the radiative term is more complex due to absorption, emission, and multiple scattering, all occurring within the PEA and affecting the radiative flux at the emitter. We thus evaluated the radiative heat flux q_{r} within the PEA by numerically solving the radiative transfer equation (RTE) using the discrete ordinate method (*35*). By independently solving for the conductive and radiative terms and iteratively evaluating the PEA temperature profile until the HTE was satisfied, the model calculates the PEA steady-state temperature profile as well as conductive and radiative heat flux at all positions within the PEA. Last, the emitter cooling power P_{cool} is calculated by summing the contribution of the conductive and radiative heat flux at the PEA/emitter boundary. Convection with the ambient air, solar irradiation, and atmospheric emission were implemented as boundary conditions at the top of the PEA, while a diffusely emitting and reflecting emitter at T_{emitter} were set as boundary conditions at the bottom of the PEA. The optical properties (scattering albedo, extinction coefficient, and scattering phase function) of the PEA needed for the RTE were experimentally determined from reflectance and transmittance measurements by solving the inverse problem (*36*). Additional details on the model are given in the Supplementary Materials.

Cooling performance enhancement using PEA

Using the developed model and experimentally determined optical properties of the PEA, we predict the cooling power of any given emitter (with known spectral optical properties and temperature), ambient conditions (which include ambient temperature, spectral atmospheric transmittance, solar irradiation, and convection coefficient with ambient air), and PEA thickness. Figure 3 shows the theoretical daytime (Fig. 3A) and nighttime (Fig. 3B) cooling power of a typical stepwise selective emitter ($R_{\mathrm{solar}} = 1 - \alpha_{\mathrm{solar}} = 0.97$; $\varepsilon_{\mathrm{IR}} = 0.9$) facing a standard atmosphere (U.S. Standard Atmosphere 1976) at different temperatures $\Delta T = T_{\mathrm{emitter}} - T_{\mathrm{amb}}$ combined with PEA of varying thickness t_{PEA}. Results show that in the absence of PEA ($t_{\mathrm{PEA}} = 0$ mm), substantial subambient temperatures ($\Delta T \lesssim 0$°C) are not achievable (i.e., $P_{\mathrm{cool}} < 0$ W/m^2) because of dominant solar heating and parasitic heat gain. However, increasing t_{PEA} reduces solar absorption and parasitic heat gain at the emitter, enabling lower temperatures (up to $\Delta T = -7$°C and $\Delta T = -11$°C for daytime and nighttime, respectively) and higher cooling powers. A maximum cooling power (indicated by the dot symbol) is also observed for each ΔT curves, highlighting the compromise between the decreasing IR transmittance and increasing solar reflectance and thermal insulation associated with thicker PEA. Furthermore, an increasing t_{PEA} for $\Delta T > 0$°C decreases P_{cool} as convection now positively contributes to the emitter cooling. In general, similar trends are observed between daytime and nighttime operation, although the nighttime performance allows us to decouple solar absorption in the PEA and emitter from the thermally insulating property of the PEA. It is also important to recognize that the results presented in Fig. 3 can be strongly influenced by the atmospheric conditions specific to a location and time such as humidity and cloud cover, and these conditions should therefore be accounted for (*19*). We thus show that lower subambient temperatures and higher cooling powers are possible for both daytime and nighttime operation when using an OSTI cover such as PEA.

Decoupling cooling performance from emitter solar reflectivity

A further advantage of using an OSTI cover is that it relaxes the requirement to use a potentially complex and costly near-ideal solar-reflecting emitter to achieve daytime radiative cooling. Adding a 20-mm-thick PEA to a black emitter reduces solar absorption by 98.9% (see fig. S2), which is better or comparable to state-of-the-art selective emitters. Furthermore, when combined with that same thickness of PEA, increasing the emitter solar reflectivity R_{solar} from 0 to 0.97 (typical of existing selective emitters) only reduces solar absorption at the emitter by a further 0.5%, meaning that the optical selectivity of the emitter is no longer critical when combined with PEA. Using an OSTI cover could thus enable the use of simpler and lower-cost emitters such as commercially available paints without compromising performance.

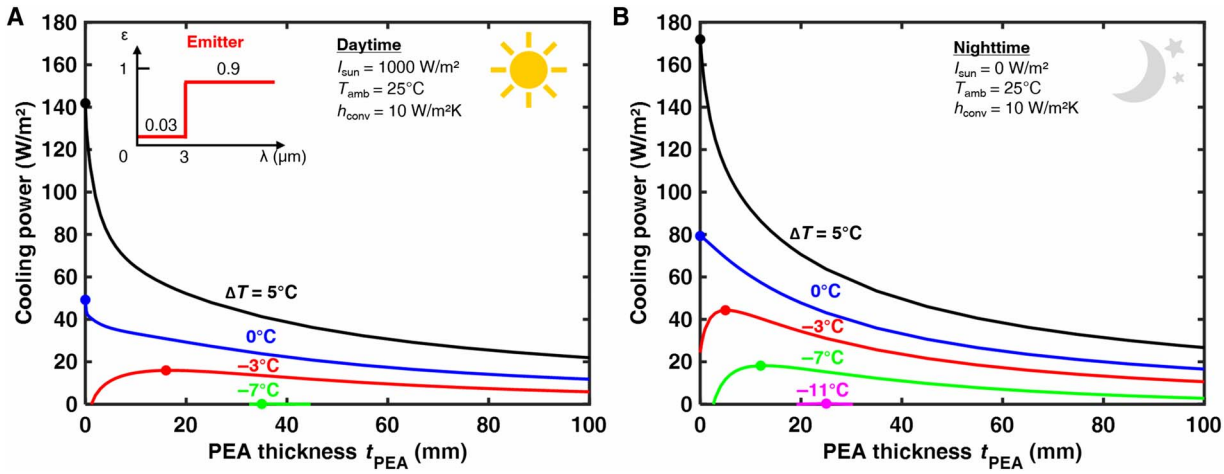

Fig. 3. Performance of radiative coolers with PEA. (**A**) Daytime cooling performance of a semi-ideal selective emitter (R_{solar} = 1 − α_{solar} = 0.97 and ε_{IR} = 0.9) at different temperatures ($\Delta T = T_{emitter} - T_{amb}$). The maximum cooling power is shown by a solid point for each emitter temperature curve. An optimal aerogel thickness exists to achieve the maximum cooling power at a given emitter temperature. The results shown were calculated based on the U.S. Standard Atmosphere 1976. Atmospheric conditions specific to a location and time, such as humidity and cloud cover, can considerably affect the results and should be accounted for accordingly (*19*). (**B**) Results for nighttime cooling performance. Higher cooling power and lower emitter temperatures can be achieved due to the absence of solar irradiation.

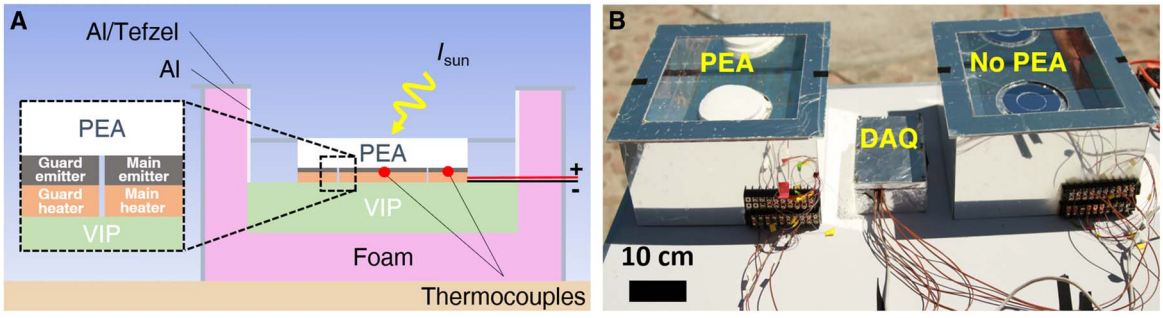

Fig. 4. Experimental setup. (**A**) Schematic of the radiative cooler. A PEA/emitter/heater assembly is placed on top of a vacuum insulation panel (VIP) that sits inside a thermally insulating foam (FOAMULAR 150) box. The box is covered with Tefzel-coated polished aluminum sheets to minimize solar heating. The emitter/heater consists of two separate parts—the main emitter/heater and the guard emitter/heater (see inset). (**B**) Picture of the setup consisting of two identical devices (left: device with PEA; right: device with no PEA). A DAQ (enclosed in an aluminum box) is also visible. More pictures showing details of the experimental location and setup are included in fig. S3. Photo credit: Arny Leroy, Massachusetts Institute of Technology.

Experimental design

We designed a proof-of-concept experimental setup (Fig. 4 and fig. S3) to simultaneously compare the performance of two radiative coolers—one with PEA and one without. Each radiative cooler had an identical 10-cm-diameter two-part selective emitter made from a 3M Enhanced Specular Reflector film on top of polished aluminum (R_{solar} = 0.942; $\varepsilon_{8–13\mu m}$ = 0.893; see fig. S4 for optical properties). The two parts of the emitter consisted of a 5-cm-diameter main emitter in the center, surrounded by a 10-cm-diameter guard emitter with a separation gap of 0.5 mm. The separation of the emitter in two parts is a similar approach to the one used in the guarded-hot-plate thermal conductivity measurement standard test method (*37*). This approach limits any 2D heat transfer effects to the guard emitter and ensures 1D heat transfer at the main emitter, thus replicating the performance of a large-scale device not affected by side losses. Heaters, as well as T-type thermocouples, were attached to the back of the (main and guard) emitters to enable control and measurement of their temperature. Power supplies were used in a four- and two-wire configuration at the main and guard heaters, respectively, for accurate measurement and control of their power consumption. A 0.5-mm-thick thermally conductive copper plate was also placed between each heater and emitter to minimize temperature gradients at the emitter. The emitter/heater assembly rested on top of a highly insulating vacuum insulation panel (VIP; Thermal Vision THRESHOLD; 23 by 23 by 5 cm; k_{VIP} = 2.9 mW/mK), which, in turn, sat at the bottom of a polystyrene foam (FOAMULAR 150) box (30 by 30 by 15 cm), minimizing the parasitic heat gains at the back side of the emitter. The horizontal surfaces of the setups were covered with Tefzel-coated aluminum to minimize parasitic solar heating of the box, and the inner vertical walls of the polystyrene foam box were covered with polished aluminum sheets to maximize the view factor between the emitter and the sky. Different thicknesses of PEA were achieved by stacking standard 6-mm-thick samples. With two identical devices in which the PEA thickness can be controlled, we were able to directly evaluate the benefits of PEA for radiative cooling and validate our theoretical model.

Experimental results

Our first experiment focused on measuring the minimum stagnation temperature of the two devices—one with 12-mm-thick PEA and one without PEA—over a full 24-hour cycle, demonstrating both the

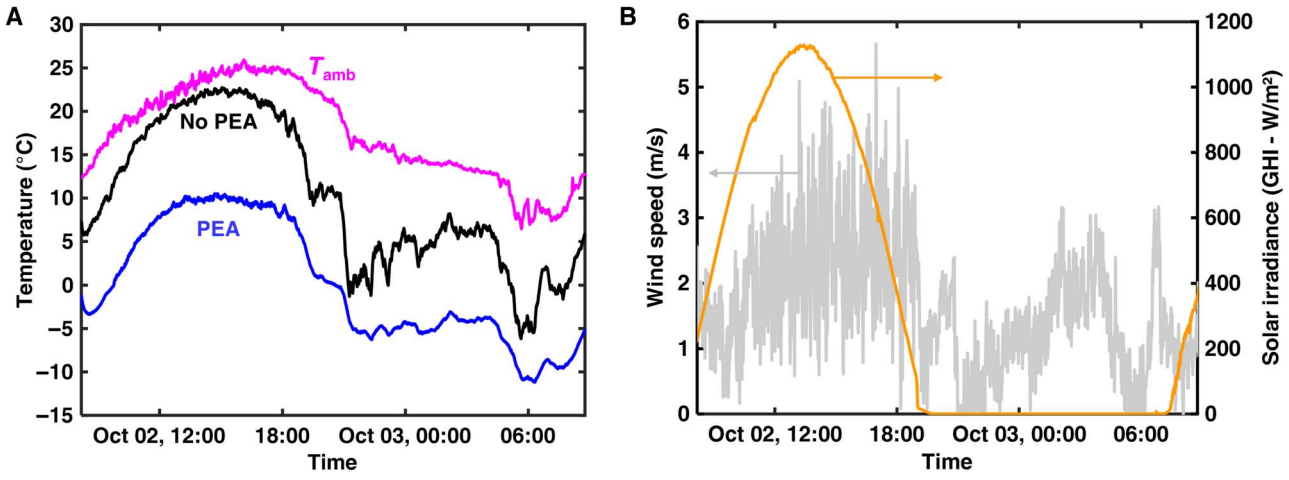

Fig. 5. Stagnation temperature of radiative cooler. (**A**) Stagnation temperature of two devices (12-mm-thick PEA and no PEA) over a 24-hour period in early October in San Pedro de Atacama, Chile. The device with the PEA achieves 13°C subambient cooling around solar noon (30-min average around 13:22; GHI = 1123 W/m^2) compared with 1.7°C without the PEA. (**B**) Wind speed and solar irradiation during the stagnation temperature experiment.

daytime and nighttime benefits of PEA. Both devices were placed next to each other and exposed to direct sunlight, as shown in Fig. 4B. Figure 5A shows the temperature of both devices (PEA and no PEA) as well as the ambient (T_{amb}) temperature during the 24-hour cycle. Figure 5B also shows the corresponding wind speed and solar GHI measured during the experiment. During that 24-hour period, the temperature of both devices closely tracked the ambient temperature and solar irradiance. However, the emitter with the PEA constantly maintained a much lower temperature than the uninsulated emitter because of the solar-reflecting and thermally insulating nature of the PEA. Around solar noon (30-min average around 13:22) at an average solar irradiance of 1123 W/m^2, a temperature difference with the ambient of $\Delta T = -13$°C was measured for the PEA device, while the no-PEA device only achieved $\Delta T = -1.7$°C. Similarly, around midnight, the PEA device achieved $\Delta T = -18.3$°C, while the no-PEA device reached $\Delta T = -8.4$°C. Moreover, the no-PEA emitter temperature was more strongly influenced by wind than the PEA emitter (see temperature fluctuations in Fig. 5A and the corresponding wind speed variations in Fig. 5B), indicating the effectiveness of the PEA to reduce parasitic heat gain by adding an extra thermal resistance between the emitter and the ambient air. The combined high solar reflectance (modeled $R_{solar} = 0.944$ for 12-mm-thick PEA) and added conduction thermal resistance ($\sim t_{PEA}/k_{PEA}$) of the PEA enabled much lower emitter stagnation temperatures during both day and night compared with an uninsulated high-performance selective emitter.

We performed a second set of experiments to evaluate and compare the useful daytime cooling power at different PEA thicknesses. In one of these experiments (Fig. 6), we compared two extreme cases, an emitter covered with a thick (18 mm) layer of PEA (PEA) against an emitter without PEA (no PEA). In another similar experiment (fig. S5), we compared two intermediate thicknesses (6-mm PEA versus 12-mm PEA), demonstrating the variation in cooling performance with PEA thickness. We started the experiments by allowing the emitters to cool down to near steady-state conditions (see the PEA and no-PEA emitter temperatures in Fig. 6A). We then increased the temperature of the (main and guard) emitters in a stepwise manner using the proportional–integral–derivative (PID) controlled heaters at their back side. At the same time, we measured the heater power at both main emitters as well as the ambient conditions (ambient temperature and humidity, wind, speed, and solar irradiance). The experimental cooling power was then obtained by normalizing the heater power, averaged over 2 min, by the main emitter area at every temperature step. More details about the cooling power experiment and the measurement uncertainty are included in Materials and Methods.

Figure 6B shows the theoretical (solid lines) and experimental (data points) emitter cooling power versus the emitter subcooling for the two devices (PEA and no PEA). The theoretical results were obtained using the model presented earlier and the atmospheric transmittance modeled based on the geographical location and the average weather conditions (see inset in Fig. 6B) during the time of the experiments (*30*). Experimentally, the cooling power of the PEA device was 96 ± 9 W/m^2 near the ambient temperature ($\Delta T = -0.6° \pm 0.8$°C) when the average solar irradiance was 936 W/m^2, compared with a cooling power of 46 ± 10 W/m^2 ($\Delta T = 0.2° \pm 0.8$°C) for the no-PEA device. Similar to the stagnation temperature experiment, the device with PEA also enabled lower subambient temperatures (maximum cooling up to $\Delta T = -15$°C compared with $\Delta T = -3.8$°C for the no-PEA emitter according to the model) due to the added solar reflectance and thermal insulation. More specifically, by adding 18 mm of PEA on top of the emitter, we were able to reduce h_{eff} from 12.9 to 1.4 W/m^{2}K, while the cover provided an additional solar reflectance $R_{solar} = 0.948$ based on our model. Overall, the experimental and theoretical results are in good agreement, demonstrating the potential of the model to predict the performance of a radiative cooler with PEA. Differences between the experimental and theoretical results can be explained by the uncertainty in the measurements, the fluctuations in the ambient conditions, and the theoretical model approximations including assuming 1D heat transfer (infinitively large emitter and PEA) and the azimuthally symmetric radiative heat transfer, which requires the solar irradiation to be normal to the emitter (see the Supplementary Materials). Additional experimental results are also presented in the Supplementary Materials: (i) In fig. S5, we demonstrate the influence of PEA thickness (6-mm PEA versus 12-mm PEA) on the emitter cooling power; (ii) in fig. S6, we demonstrate the radiative cooling performance (stagnation temperature and cooling power) in a more humid and colder environment (Cambridge, Massachusetts); (iii) in fig. S7, we demonstrate the influence of emitter solar reflectance (black

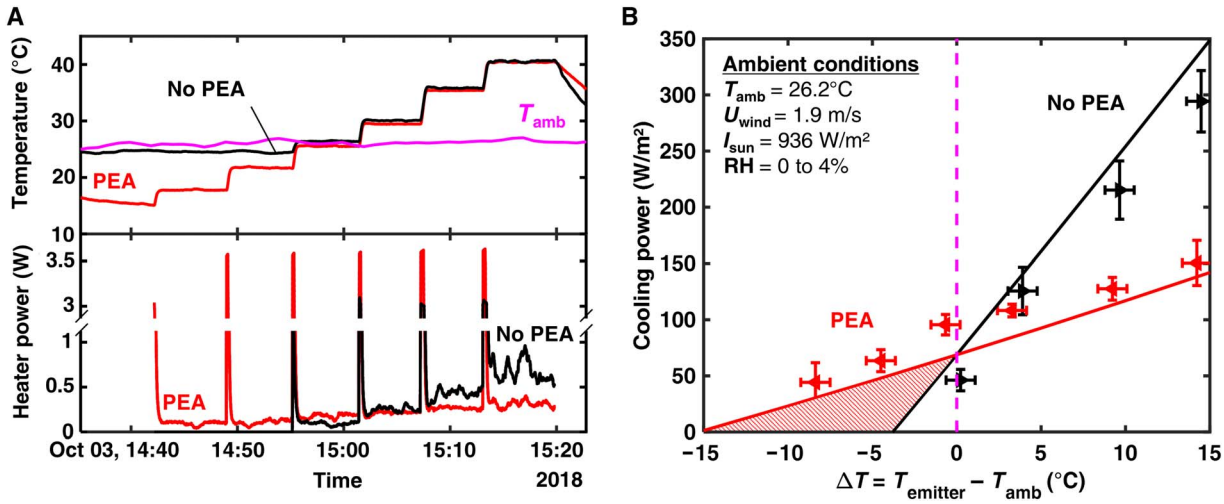

Fig. 6. Cooling performance of radiative cooler. (**A**) Measured emitter temperature of two devices (18-mm-thick PEA and no PEA) as well as the corresponding heater power and ambient temperature during the cooling power experiment. (**B**) Cooling power of the two devices as a function of the emitter subcooling in San Pedro de Atacama, Chile. The shaded area represents the range of cooling power and subambient temperatures made accessible by the PEA compared with an uninsulated emitter.

versus selective emitter) on the radiative cooling performance (temperature and cooling power) when covered with 18-mm-thick PEA. These results further show good agreement with the model in two different regions of the world while also suggesting that PEA greatly minimizes the importance of the emitter solar reflectivity and that an optimal PEA thickness (i.e., maximizing cooling power) exists for a given subambient temperature. By using PEA for radiative cooling, we enabled higher subambient cooling power and operation at much lower temperatures than with an uninsulated selective emitter, opening up a wide regime of operation (shaded area in Fig. 6B) that enables access to cooling powers and subambient temperatures that were previously not accessible.

DISCUSSION

We developed and experimentally demonstrated the use of an OSTI PEA cover for high-performance subambient radiative cooling. By adding PEA on top of a radiative cooling emitter, we provided a simple approach to reducing parasitic heat gain and solar absorption at the emitter, two limiting factors that have severely hindered the performance of previous experimental demonstrations. Using PEA and a commercially available selective emitter, we experimentally demonstrated a daytime cooling power of 96 W/m^2 at ambient temperature as well as cooling of up to 13°C below ambient, surpassing by more than 22% the performance of previous stagnation temperature experiments (*19*).

In parallel to our experiments, we also investigated the performance of PEA using a robust theoretical model considering both conductive and radiative heat transfer. The model provided us with insights into the compromise between system performance and PEA thickness, which allowed us to determine an optimal PEA thickness for any given system, weather conditions, and operating temperature. We have also demonstrated that because of its high solar reflectance, PEA allowed the use of nonselective emitters with negligible degradation in performance, possibly enabling simpler-design and lower-cost radiative coolers.

We believe our work has proven the potential of OSTI covers for subambient radiative cooling. Because the approach is modular and can readily be implemented in existing systems, our work can help improve the performance of existing radiative cooling systems such as radiative cooling water panels for air conditioning units of buildings (*16*, *19*), sorption-based water harvesting devices (*38*), as well as passive refrigeration of food produce (*39*). Last, new research opportunities that will further enhance the performance of radiative coolers will stem from this work. Among these opportunities, alternative IR-transparent materials, such as BaF_2 and ZnS (*18*), could be explored to achieve better optical and thermal performance, and further development of the theoretical models to optimize the cover thickness and optical properties for varying weather conditions (e.g., day-to-day variation over a year) as well as costs (e.g., incremental increase in performance versus incremental cost with thicker PEA) is still required.

MATERIALS AND METHODS

Fabrication of PEAs

Ultrahigh–molecular weight polyethylene [0.5 weight % (wt %); 429015, Sigma-Aldrich; polymer] was mixed with 99.3 wt % of paraffin oil (76235, Sigma-Aldrich; solvent) and 0.2 wt % of butylated hydroxytoluene (W218405, Sigma-Aldrich; antioxidant) in a sealed beaker at room temperature. The solution was then heated in a silicone oil bath at 150°C and mixed using a magnetic stirrer. After complete dissolution of the polymer in the solvent (~30 min), the homogeneous solution was poured in a preheated circular aluminum mold (13.5-cm diameter and 10-mm depth). The mold was then inserted in a water bath (5°C), initiating the TIPS and resulting in a polymer gel. Next, the paraffin oil was removed using a three-step solvent exchange in hexane. Another three-step solvent exchange in ethanol was performed to remove the hexane, a necessary step to ensure chemical compatibility with our critical point dryer. Last, the gel was dried using a critical point dryer (Automegasamdri-938, Tousimis), which replaced the ethanol from the PEA with air while preventing collapse of the porous structure. The initial polymer concentration was chosen to maximize solar reflectivity, IR transmittance, and structural integrity of the gel during fabrication, while the sample thickness was chosen as a compromise between number of samples needed for the experiments to achieve the desired thicknesses and fabrication time (i.e., solvent exchange and critical point drying are diffusion-limited processes).

Density measurement

The density of the PEA was calculated from its measured volume and mass. The reported density was determined from the average density of three samples, and the uncertainty accounts for the accuracy of the measured mass and volume, as well as variation between samples.

Thermal conductivity measurement

A thermal conductivity setup based on the guarded-hot-plate method ASTM C1044-16 (*37*) was used to measure the thermal conductivity of the PEA. Similar to the emitter in the radiative cooling experiments, a main heater (7-cm diameter) and a surrounding guard heater (14-cm diameter) were used in this standard measurement. This design limits 2D heat transfer effects to the guard heater, allowing 1D heat transfer at the main heater, which thus mimics a large sample where side effects are negligible. Only the main heater power and area were used in the characterization of the sample thermal conductivity. Polished copper was used as the boundary surface of the heater and cold plate to minimize radiative heat transfer between the two through the PEA, thus allowing measurement of the conductive and convective components of thermal conductivity of the porous material. Tests at four different temperature differences (2.5°, 5°, 10°, and 20°C), all with an average temperature of 20°C, were performed and averaged. The reported uncertainty in the measured thermal conductivity accounts for the measurement accuracy of the sample thickness, temperature difference, heater surface area, and heater power, as well as the variation between tests.

Optical measurements

The optical transmittance and reflectance of the PEA and the emitter were measured using an ultraviolet–visible–near-infrared spectrophotometer (Cary 4000, Agilent) and an Fourier transform infrared spectrometer. Integrating spheres [Internal DRA-2500 (Agilent) and Mid-IR IntegratIR (Pike Technologies), respectively] were used to account for the diffusely transmitted and reflected light.

Ambient weather measurement

A Campbell Scientific CS215 probe was used to measure the ambient temperature (accuracy of ±0.4°C between 5° and 40°C) and relative humidity (accuracy of ±4% between 0 and 100%). The wind speed was measured using an anemometer (034B, Met One) with an uncertainty of 0.1 m/s within the wind speed range of our experiment. The GHI solar irradiance was measured using a pyranometer (CMP6, Kipp & Zonen) with an uncertainty of ±2.3%. A rotating shadowband radiometer (RSR2, Campbell Scientific equipped with an LI-200R, LI-COR photovoltaic pyranometer) was also used as a backup irradiance measurement system and was in excellent agreement with the pyranometer. All instruments were connected to a datalogger (CR1000, Campbell Scientific). All weather data were sampled every 3 s and averaged every minute.

Stagnation temperature measurement

The temperature of the emitters was measured using T-type thermocouples (TT-T-40-SLE-25, Omega) installed at their back side (center of the main and guard) and connected to a DAQ module (USB-TC, Measurement Computing). The DAQ was enclosed in a reflective aluminum box to minimize temperature gradients between the thermocouple junctions and the DAQ cold junction sensors. The thermocouples were calibrated before the experiments in an ethylene glycol solution using a chiller (A25, Thermo Scientific) and a resistance temperature detector (P-M-A-1/4-3-1/2-PS-12, Omega), which resulted in an uncertainty of ±0.3°C. The data acquisition was done using LabVIEW.

Cooling power measurement

The temperature of the emitters was controlled using heaters (main and guard, like the guarded-hot-plate thermal conductivity setup) at their back side that were regulated using a PID control. Each main heater was connected to a power supply (2425 Keithley and 2440 Keithley) in a four-wire configuration to allow accurate measurement of the heating power at the emitter only. A triple-channel power supply (2230-30-1, Keithley) was also used to power the guard heaters in a two-wire configuration. The data acquisition and PID control were accomplished using LabVIEW. The main heater power and emitter temperature were averaged for 2 min after the initial transient peak in heater power. The uncertainty of the emitter temperature was determined from the thermocouple and ambient temperature sensor accuracy, as well as their fluctuations during the averaging period (2-min average after stabilization of the emitter temperature). The cooling power uncertainty was determined after accounting for the accuracy of the main emitter area measurement and of the power supplies, the main heater power fluctuations during the averaging period, as well as the small parasitic lateral heat transfer between the main and guard emitters. Specifically, we performed an indoor measurement to characterize the lateral heat transfer coefficient between the main and guard emitters and found it to be 24.5 W/m^2K, meaning that for every degree in temperature difference, an effective change in cooling power of 24.5 W/m^2 was observed at the main emitter. This effect was, however, only found to be important near the stagnation temperature of the devices. Because of higher parasitic heat gain and low cooling power close to the stagnation temperature, the guard temperature was higher than the main emitter, causing heat transfer between the two emitters and giving rise to additional 2D parasitic heat gains at the main emitter. Since all other data points and the model assumed 1D heat transfer at the main emitter, the cooling power data point at the stagnation temperature of both devices was removed.

SUPPLEMENTARY MATERIALS

Supplementary material for this article is available at http://advances.sciencemag.org/cgi/content/full/5/10/eaat9480/DC1

Influence of emitter solar reflectivity and effective heat transfer coefficient
Theoretical model for emitter cooling power
Optical properties of PEA
Fig. S1. Influence of system nonidealities.
Fig. S2. Solar absorption at the emitter.
Fig. S3. Experimental setup.
Fig. S4. Selective emitter emissivity.
Fig. S5. Influence of PEA thickness.
Fig. S6. Cooling performance of radiative cooler in Cambridge, Massachusetts.
Fig. S7. Experimental comparison of selective and black emitters with PEA.
Fig. S8. Iterative process for cooling power modeling.
Fig. S9. Optical properties of PEA.
Reference (*40*)

REFERENCES AND NOTES

1. International Energy Agency, "The Future of Cooling: Opportunities for energy- efficient air conditioning" (2018); https://webstore.iea.org/the-future-of-cooling.
2. J. A. Foley, N. Ramankutty, K. A. Brauman, E. S. Cassidy, J. S. Gerber, M. Johnston, N. D. Mueller, C. O'Connell, D. K. Ray, P. C. West, C. Balzer, E. M. Bennett, S. R. Carpenter, J. Hill,

C. Monfreda, S. Polasky, J. Rockström, J. Sheehan, S. Siebert, D. Tilman, D. P. M. Zaks, Solutions for a cultivated planet. *Nature* **478**, 337–342 (2011).
3. F. Trombe, Perspectives sur l'utilisation des rayonnements solaires et terrestres dans certaines régions du monde. *Rev. Gén. Therm.* **6**, 1285–1314 (1967).
4. A. W. Harrison, M. R. Walton, Radiative cooling of TiO_2 white paint. *Sol. Energy.* **20**, 185–188 (1978).
5. A. Hjortsberg, C. G. Granqvist, Radiative cooling with selectively emitting ethylene gas. *Appl. Phys. Lett.* **39**, 507–509 (1981).
6. E. M. Lushiku, A. Hjortsberg, C. G. Granqvist, Radiative cooling with selectively infrared-emitting ammonia gas. *J. Appl. Phys.* **53**, 5526–5530 (1982).
7. A. R. Gentle, G. B. Smith, Radiative heat pumping from the Earth using surface phonon resonant nanoparticles. *Nano Lett.* **10**, 373–379 (2010).
8. L. Zhu, A. Raman, S. Fan, Color-preserving daytime radiative cooling. *Appl. Phys. Lett.* **103**, 223902 (2013).
9. A. P. Raman, M. A. Anoma, L. Zhu, E. Rephaeli, S. Fan, Passive radiative cooling below ambient air temperature under direct sunlight. *Nature* **515**, 540–544 (2014).
10. A. R. Gentle, G. B. Smith, A subambient open roof surface under the mid-summer sun. *Adv. Sci.* **2**, 1500119 (2015).
11. L. Zhu, A. P. Raman, S. Fan, Radiative cooling of solar absorbers using a visibly transparent photonic crystal thermal blackbody. *Proc. Natl. Acad. Sci. U.S.A.* **112**, 12282–12287 (2015).
12. Z. Chen, L. Zhu, A. Raman, S. Fan, Radiative cooling to deep sub-freezing temperatures through a 24-h day–night cycle. *Nat. Commun.* **7**, 13729 (2016).
13. Y. Zhai, Y. Ma, S. N. David, D. Zhao, R. Lou, G. Tan, R. Yang, X. Yin, Scalable-manufactured randomized glass-polymer hybrid metamaterial for daytime radiative cooling. *Science* **355**, 1062–1066 (2017).
14. A. R. Gentle, A. Nuhoglu, M. D. Arnold, G. B. Smith, in *Thermal Radiation Management for Energy Applications*, M. M. Al-Jassim, P. Bermel, Eds. (SPIE, 2017); https://www.spiedigitallibrary.org/conference-proceedings-of-spie/10369/2274568/3D-printable-optical-structures-for-sub-ambient-sky-cooling/10.1117/12.2274568.full, p. 10.
15. J.-l. Kou, Z. Jurado, Z. Chen, S. Fan, A. J. Minnich, Daytime radiative cooling using near-black infrared emitters. *ACS Photonics* **4**, 626–630 (2017).
16. E. A. Goldstein, A. P. Raman, S. Fan, Sub-ambient non-evaporative fluid cooling with the sky. *Nat. Energy.* **2**, 17143 (2017).
17. B. Bhatia, A. Leroy, Y. Shen, L. Zhao, M. Gianello, D. Li, T. Gu, J. Hu, M. Soljačić, E. N. Wang, Passive directional sub-ambient daytime radiative cooling. *Nat. Commun.* **9**, 5001 (2018).
18. H. Kim, A. Lenert, Optical and thermal filtering nanoporous materials for sub-ambient radiative cooling. *J. Opt.* **20**, 084002 (2018).
19. D. Zhao, A. Aili, Y. Zhai, J. Lu, D. Kidd, G. Tan, X. Yin, R. Yang, Subambient cooling of water: Toward real-world applications of daytime radiative cooling. *Joule* **3**, 111–123 (2019).
20. H. Kim, A. Lenert, in *Proceedings of the 16th International Heat Transfer Conference* (IHTC, 2018), China National Convention Center, Beijing, China, August 10-15, 2018, pp. 1–8.
21. P. Yang, C. Chen, Z. M. Zhang, A dual-layer structure with record-high solar reflectance for daytime radiative cooling. *Sol. Energy.* **169**, 316–324 (2018).
22. J. Mandal, Y. Fu, A. C. Overvig, M. Jia, K. Sun, N. N. Shi, H. Zhou, X. Xiao, N. Yu, Y. Yang, Hierarchically porous polymer coatings for highly efficient passive daytime radiative cooling. *Science* **362**, 315–319 (2018).
23. B. Zhao, M. Hu, X. Ao, N. Chen, G. Pei, Radiative cooling: A review of fundamentals, materials, applications, and prospects. *Appl. Energy* **236**, 489–513 (2019).
24. L. Zhu, A. Raman, K. X. Wang, M. A. Anoma, S. Fan, Radiative cooling of solar cells. *Optica* **1**, 32–38 (2014).
25. Z. Chen, L. Zhu, W. Li, S. Fan, Simultaneously and synergistically harvest energy from the sun and outer space. *Joule*, 101–110 (2019).
26. N. A. Nilsson, T. S. Eriksson, C. G. Granqvist, Infrared-transparent convection shields for radiative cooling: Initial results on corrugated polyethylene foils. *Sol. Energy Mater.* **12**, 327–333 (1985).
27. A. R. Gentle, K. L. Dybdal, G. B. Smith, Polymeric mesh for durable infra-red transparent convection shields: Applications in cool roofs and sky cooling. *Sol. Energy Mater. Sol. Cells.* **115**, 79–85 (2013).
28. S. N. Bathgate, S. G. Bosi, A robust convection cover material for selective radiative cooling applications. *Sol. Energy Mater. Sol. Cells.* **95**, 2778–2785 (2011).
29. M. Benlattar, E. M. Oualim, T. Mouhib, M. Harmouchi, A. Mouhsen, A. Belafhal, Thin cadmium sulphide film for radiative cooling application. *Opt. Commun.* **267**, 65–68 (2006).
30. A. Berk, P. Conforti, R. Kennett, T. Perkins, F. Hawes, J. van den Bosch, in *Proceeding of SPIE 9088, Algorithms and Technologies for Multispectral, Hyperspectral, and Ultraspectral Imagery XX*, M. Velez-Reyes, F. A. Kruse, Eds. (2014); http://proceedings.spiedigitallibrary.org/proceeding.aspx?doi=10.1117/12.2050433, p. 90880H.
31. J. V. Gulmine, P. R. Janissek, H. M. Heise, L. Akcelrud, Polyethylene characterization by FTIR. *Polym. Test.* **21**, 557–563 (2002).
32. P.-C. Hsu, A. Y. Song, P. B. Catrysse, C. Liu, Y. Peng, J. Xie, S. Fan, Y. Cui, Radiative human body cooling by nanoporous polyethylene textile. *Science* **353**, 1019–1023 (2016).
33. Y. A. Attia, Polyethylene aerogels and method of their production, US9034934B1 (2015), p. 11.
34. C. Daniel, S. Longo, G. Guerra, High porosity polyethylene aerogels. *Polyolefins J.* **2**, 49–55 (2015).
35. K. Stamnes, G. E. Thomas, J. J. Stamnes, *Radiative Transfer in the Atmosphere and Ocean* (Cambridge Univ. Press, Cambridge, 2017); http://ebooks.cambridge.org/ref/id/CBO9781316148549.
36. L. Zhao, S. Yang, B. Bhatia, E. Strobach, E. N. Wang, Modeling silica aerogel optical performance by determining its radiative properties. *AIP Adv.* **6**, 025123 (2016).
37. ASTM International, "ASTM C1044-16 Standard Practice for Using a Guarded-Hot-Plate Apparatus or Thin-Heater Apparatus in the Single-Sided Mode" (West Conshohocken, PA, 2016).
38. Y. Tu, R. Wang, Y. Zhang, J. Wang, Progress and expectation of atmospheric water harvesting. *Joule* **2**, 1452–1475 (2018).
39. C. I. Ezekwe, Performance of a heat pipe assisted night sky radiative cooler. *Energy Convers. Manag.* **30**, 403–408 (1990).
40. E. Sartori, Convection coefficient equations for forced air flow over flat surfaces. *Sol. Energy.* **80**, 1063–1071 (2006).

Acknowledgments: We thank E. Strobach for help with the fabrication of the PEA. We also thank R. Escobar for sharing instrumentation for solar radiation and weather measurements. **Funding:** A.L., B.B. and C.C.K. as well as the experiments were supported by the Solid-State Solar Thermal Energy Conversion (S3TEC) Center, an Energy Frontier Research Center funded by the U.S. Department of Energy, Office of Science, Basic Energy Sciences under award no. DE-FG02-09ER46577. A.M.G., M.D.C.H. A.C.-C. as well as travel to Chile were supported by the MIT International Science and Technology Initiatives (MISTI) Chile Global Seed Funds (GSF) grant "Design and Benchmark of a Hybrid Thermophotovoltaic HTPV Energy Conversion System for Heat Recovery and Management" and by the MIT International Science and Technology Initiatives - Pontificia Universidad Católica (MISTI-PUC) Global Seed Funds (GSF) grant "Thermophotovoltaic (TPV)-based Hybrid System for Energy Conversion, Waste Heat Recovery and Water Purification." **Author contributions:** A.L. and B.B. conceptualized the work and fabricated the experimental setup. A.L. and L. Zhao fabricated the PEA samples. A.L., B.B., and C.C.K. conducted the experiments. M.D.C.H., A.C.-C., and A.M.G. organized the trip to San Pedro de Atacama. A.C.-C. and M.D.C.H. performed the ambient weather measurements. A.L. and B.B. optically characterized the materials. A.L., L. Zhao, and L. Zhang conducted the theoretical modeling. A.L. wrote the paper with input from all authors. A.M.G. and E.N.W. supervised and guided the project. **Competing interests:** The authors declare that they have no competing interests. **Data and materials availability:** All data needed to evaluate the conclusions in the paper are present in the paper and/or the Supplementary Materials. Additional data related to this paper may be requested from the authors.

Submitted 23 April 2019
Accepted 17 September 2019
Published 30 October 2019
10.1126/sciadv.aat9480

Citation: A. Leroy, B. Bhatia, C. C. Kelsall, A. Castillejo-Cuberos, M. Di Capua H., L. Zhao, L. Zhang, A. M. Guzman, E. N. Wang, High-performance subambient radiative cooling enabled by optically selective and thermally insulating polyethylene aerogel. *Sci. Adv.* **5**, eaat9480 (2019).

Science Advances

High-performance subambient radiative cooling enabled by optically selective and thermally insulating polyethylene aerogel

A. Leroy, B. Bhatia, C. C. Kelsall, A. Castillejo-Cuberos, M. Di Capua H., L. Zhao, L. Zhang, A. M. Guzman and E. N. Wang

Sci Adv **5** (10), eaat9480.
DOI: 10.1126/sciadv.aat9480